2,7-Diaminofluorene-Based Organic Dyes for Dye-Sensitized Solar Cells: Effect of Auxiliary Donor on Optical and Electrochemical Properties

Abhishek Baheti,[†] Prachi Singh,[†] Chuan-Pei Lee,[‡] K. R. Justin Thomas,[*,†] and Kuo-Chuan Ho[‡]

[†]Organic Materials Lab, Department of Chemistry, Indian Institute of Technology Roorkee, Roorkee-247 667, India
[‡]Department of Chemical Engineering, National Taiwan University, Taipei 10617, Taiwan

S *Supporting Information*

ABSTRACT: New organic dyes containing a diarylaminofluorene unit as an electron donor and cyanoacrylic acid as acceptor and anchoring group in a donor-π-donor-π-acceptor architecture have been synthesized and characterized as sensitizers for nanocrystalline TiO$_2$-based dye-sensitized solar cells. They have shown three major electronic absorptions originating from the $\pi-\pi^*$ and charge-transfer transitions covering the broad visible range (250–550 nm) in solution. The charge-transfer transition of the dyes exhibited negative solvatochromism, suggesting a polarized ground state. They have also displayed acidochromism in solution owing to the presence of a protonation–deprotonation equilibrium. On comparison with the triphenylamine and carbazole-based parent dyes (E)-2-cyano-3-(4-(diphenylamino)phenyl)acrylic acid and (E)-2-cyano-3-(9-ethyl-9H-carbazol-3-yl)acrylic acid they exhibited longer wavelength absorptions and facile oxidation, indicating the stronger electron-donating ability of the auxiliary chromophores. In addition, they exhibited nearly two times larger light-to-electron conversion efficiency under simulated AM 1.5 G irradiation (100 mW cm^{-2}) with an aperture mask when compared to the parent dyes. Among the new dyes, the one containing the naphthylphenylamine segment showed better device characteristics attributable to the higher HOMO energy level which probably facilitates the regeneration of the dye and effective suppression of the back reaction of the injected electrons with the I$_3^-$ in the electrolyte. The optical properties of the dyes were modeled using TDDFT simulations employing different theoretical models (B3LYP, CAM-B3LYP, and MPW1K), and the best correlations with the observed parameters have been found for CAM-B3LYP and MPW1K calculations. The electron lifetimes extracted from the electrochemical impedance measurements of the dye-sensitized solar cells were used to interpret the solar cell efficiency alternations.
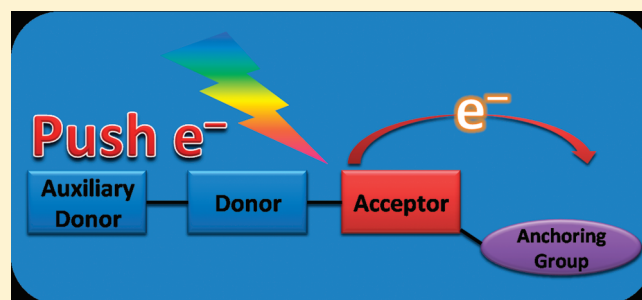
INTRODUCTION

Organic dyes capable of absorbing a visible light have received immense attention since the first report in 1991 by Grätzel and co-workers[1] on nanocrystalline anatase TiO$_2$-based dye-sensitized solar cells (DSSCs) as potential alternatives to traditional silicon-based inorganic photovoltaic devices. These cells are usually constructed using wide band gap semiconductor oxides such as TiO$_2$, a molecular sensitizer, and a redox electrolyte. Recent research has been focused on the methods to optimize the light-harvesting ability of the sensitizers and to realize a more robust electrolyte system.[2–6] Also, interest for organic dyes as an alternative to noble metal complexes has increased because of their many advantages, such as diversity of molecular structures, high molar extinction coefficient, simple synthesis, as well as low cost and environmental friendliness. Metal-free organic dyes based on triphenylamine, fluorene, thiophene, indoline, merocyanine, coumarin, etc. have been developed and found to exhibit promising device characteristics.[7] Despite the intensive efforts by materials chemists to achieve an efficient organic dye, the DSSCs based on Ru complexes

such as N3 and N719 have remained as the best commercial dyes showing solar energy-to-electricity conversion efficiency up to 11% at simulated AM 1.5 G irradiation.[8] Thus, research toward the development of organic dyes and understanding the structure–property relationship in organic dyes has been undertaken with keen interest. Organic dyes probably suffer from several competing deactivating processes of the excited state in addition to its shorter lifetime. Prolongation of the excited state either by the inducement of triplet character or introduction of energy transferring chromophores may enhance the light-harvesting capability of the dyes.

In this work, we have studied the changes in the optical and electrochemical properties of organic dyes due to the incorporation of an auxiliary electron donor featuring diphenylaminofluorene segment. We have chosen this chromophore for the following reasons: Fluorene-based organic dyes are attractive because of their high molar extinction absorption and easy functionalization

Chart 1. Structures of the Dyes
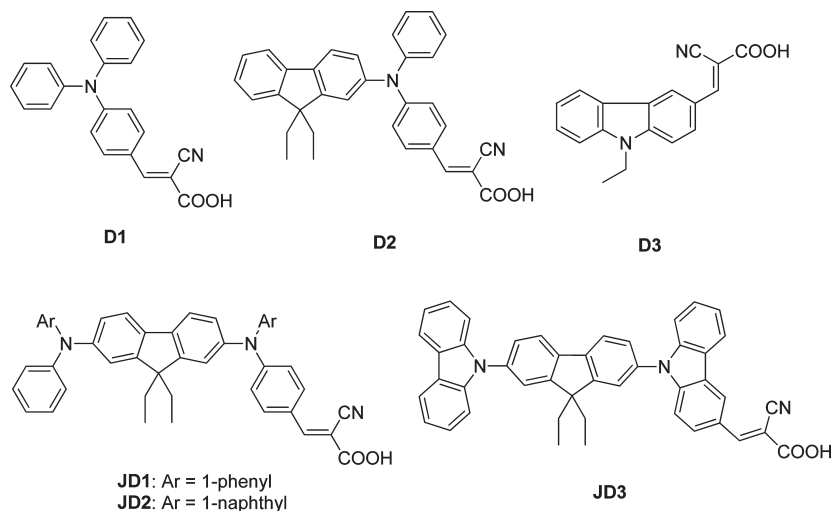
by simple chemical modifications.[7] In addition, since fluorene is an electron-rich moiety, it enhances the redox stability of the organic dyes. Substitution of the fluorene moiety in place of a phenyl group in triarylamines has been found to reduce the oxidation potential because of the electron-richness of the fluorene unit. It is hypothesized that the promising changes expected in the optical and redox properties due to the introduction of the diphenylaminofluorene unit will play a beneficial role on the light-harvesting properties of the dyes. Thus, we demonstrate in this work, by suitable chemical modification a simple triphenylamine derived organic dye, that (E)-2-cyano-3-(4-(diphenylamino)phenyl)acrylic acid (**D1**) showing an efficiency of ∼2.5%[9] can be improved significantly. Consequently, we have developed four new dyes (CHART 1) by substituting one or more of the phenyl groups in **D1** with fluorene or diarylaminofluorene and related chromophores. It is expected that the replacement of phenyl groups in **D1** with fluorene or diarylaminofluorene would enhance the donor strength of the amino unit and alter the optical and electrochemical properties of the resulting dyes. Modification in the absorption properties or redox propensity of the dyes is believed to enhance the current density and retard the back reaction of the injected electrons with the electrolyte or the oxidized dye, which could lead to efficient DSSCs.

■ RESULTS AND DISCUSSION

Synthesis and Characterization. The dyes (**D2, JD1−JD3**) were synthesized in two steps involving the formylation of the corresponding triarylamines (**1a−d**) followed by the Knoevenagel condensation of the resulting aldehydes (**2a−d**) with cyanoacetic acid (Scheme 1). The carbazole-containing dye **JD3** was synthesized by utilizing the same methodology from 9,9′-(9,9-diethyl-9H-fluorene-2,7-diyl)bis(9H-carbazole) (not shown in Scheme 1). The dyes were thoroughly characterized by ^{1}H and ^{13}C NMR and mass spectral methods. They are dark red and moderately soluble in solvents such as dichloromethane, acetonitrile, methanol, tetrahydrofuran, toluene, etc.

Optical Properties. The absorption spectra of the dyes recorded in dichloromethane are displayed in Figure 1, and the related photophysical data are summarized in Table 1. All of the dyes exhibited three absorption peaks, and the prominent red-shifted band appearing in the range of 400−550 nm is assigned to a charge-transfer
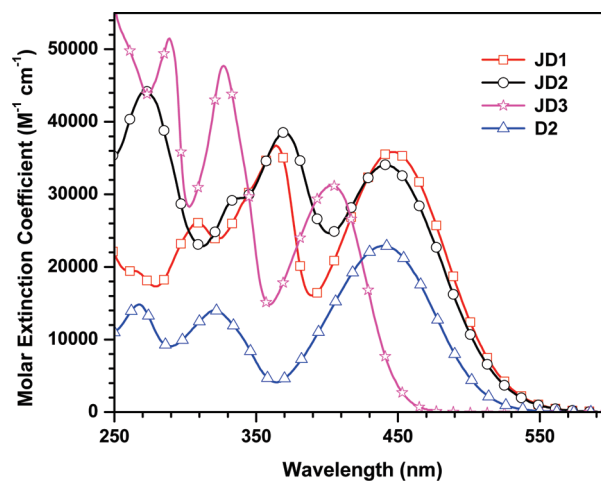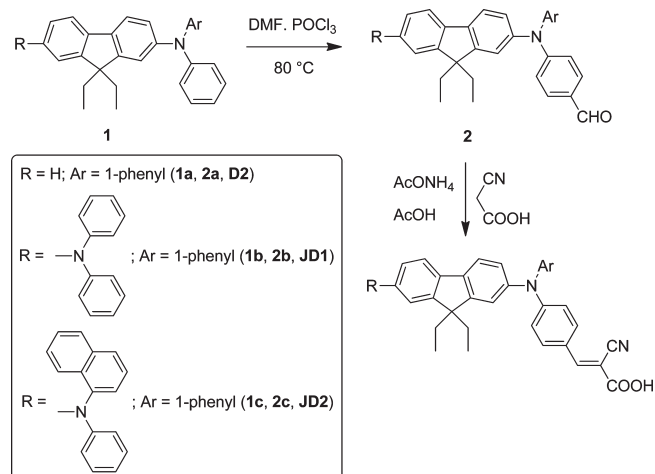
Scheme 1. Synthesis of the Dyes D2, JD1, and JD2

Figure 1. Absorption spectra of the dyes (**D2, JD1−JD3**) recorded in dichloromethane.

Table 1. Optical and Electrochemical Properties of the Dyes and Related Compounds in Dichloromethane Solution

compd	λ_{max}, nm (ε_{max}, M^{-1} cm^{-1} × 10^3)	E_{ox}, mV (ΔE_{p}, mV)[a]	HOMO,[b] eV	E_{0-0},[c] eV	LUMO,[d] eV
1a	347 (25.2), 264 (10.5)	397 (83)	5.197	3.263	1.934
1b	374 (40.2), 309 (27.9)	156 (70), 465 (67)	4.956	3.085	1.871
1c	372 (44.0), 270 (25.6)	154 (68), 495 (73)	4.954	2.913	2.041
1d	334 (39.2), 293 (41.7)	796, 1014	5.596	3.415	2.181
2a	372 (24.6), 331 (18.8)	551 (82)	5.351	2.897	2.454
2b	377 (47.9)	269 (67), 524 (71)	5.069	2.808	2.261
2c	377 (45.9)	272 (68), 559 (68)	5.072	2.793	2.279
2d	340 (42.2), 294 (45.7)	820, 1027	5.620	3.328	2.292
D2	440 (22.9), 320 (14.0), 267 (14.8)	570 (75)	5.370	2.389	2.980
JD1	447 (35.8), 370 (38.5), 309 (26.1)	263 (53), 518 (81)	5.063	2.288	2.775
JD2	441 (34.1), 370 (38.5), 272 (44.2)	233 (64), 557 (84)	5.033	2.326	2.707
JD3	403 (31.3), 327 (47.7), 289 (51.5)	838, 964	5.638	2.696	2.942

[a] Redox potentials are reported with reference to the ferrocene internal standard. [b] Deduced from the oxidation potential using the formula HOMO = 4.8 + E_{ox}. [c] Calculated from optical edge. [d] Obtained from the optical band gap and the electrochemically deduced HOMO value.

transition between the amine and cyanoacrylic segments. The absorption maximum realized for the dye **D2** is bathochromically shifted when compared to the parent dye (*E*)-2-cyano-3-(4-(diphenylamino)phenyl)acrylic acid (**D1**, 400 nm).[9] This clearly establishes the electron-richness of the fluorene segment, which enhances the donor strength of the amine segment to result in a pronounced donor—acceptor interaction. Among the dyes, the compound containing the diphenylamine unit (**JD1**) displays the red-shifted absorption profile, while the carbazole-based dye (**JD3**) possesses the blue-shifted peak. The relatively shorter wavelength peak observed for the dye **JD3** in the series is indicative of the reduced donor strength of the carbazole segment when compared to the other triarylamine units. However, the absorption peak **JD3** is red-shifted when compared to the parent compound (*E*)-2-cyano-3-(9-ethyl-9*H*-carbazol-3-yl)acrylic acid (**D3**, 385 nm)[10] suggesting an enhancement in the donor strength because of the presence of an additional electron-rich fluorenylcarbazole unit.

The role of the donor—acceptor interactions on the electronic spectra is clearly evident on comparing the absorption maxima of the parent amines, **1a—d**, and the aldehydes, **2a—d**, with that of the dyes, **D2** and **JD1—JD3** (see Table 1). For a similar structure, the absorption wavelength shifts to the low energy region on introduction of aldehyde or cyanoacrylic acid segment on the amine. The interesting feature of the absorption spectra of the dyes (**JD1—JD3**) is the additional intense bands appearing in the lower wavelength region (250—400 nm) when compared to the parent compounds **D1—D3**. These lower wavelength absorptions originate from the $\pi-\pi^*$ transitions localized within fluorene and aminofluorene segments.[11] The energies of these bands in the dyes assume the order **JD2 < JD1 < JD3** indicating the auxochromic effect due to the arylamine segments.[12]

The molar extinction coefficients of the dyes **D2** and **JD1—JD3**, at the maximum absorption of the charge-transfer transition in dichloromethane, range from 22900 to 35800 M^{-1} cm^{-1}, which are higher than those observed for the dyes **D1** (15800 M^{-1} cm^{-1})[9] and **D3** (22900 M^{-1} cm^{-1}).[10] The optical density measured for these dyes are also significantly higher than those of the Ru dyes **N3** (16000 M^{-1} cm^{-1}) and **N719**. It is noteworthy that the incorporation of additional fluorene or aminofluorene segment not only red shifts the absorption edge but also increases the molar extinction coefficient, which is highly desirable for large photocurrent generation.

All of the dyes showed negative solvatochromism for the higher wavelength absorption band when recorded in solvents of different polarity (Table 2 and Figure 2). Most red-shifted absorption was observed for dichloromethane (DCM), and the absorption peak shifted to lower wavelength on increasing the polarity (Figure 3). This is probably due to the more efficient solvation of the dyes in the polar solvents. This also confirms the charge-transfer nature for this electronic transition. In dichloromethane, all of the dyes exhibited an unexpected red-shift while in tetrahydrofuran a prominent blue shift was observed. Unusual red-shift in absorption in dichloromethane has been identified earlier for cationic dyes and attributed to the instant stabilization due to a fast rearrangement of polarizable electrons during excitation.[13] The unusual blue shift observed for the dyes in tetrahydrofuran solutions is intriguing. It is probable that the hydrogen bonding interactions of carboxylic acid unit with the tetrahydrofuran oxygen may result in a partial deprotonation. This could in turn reduce the donor—acceptor interaction in the dye and produce a blue shift in absorption.[14] Addition of TFA to the THF solutions caused the red-shift supporting the above hypothesis. Even though such hydrogen bonding possibilities are present in methanolic solution, because of the available proton population in the solution, the equilibrium might be shifted toward the acidic form.

The presence of acid—base equilibria in solution is further confirmed by the addition of trifluoroacetic acid (TFA) to the dye solutions in toluene, methanol, and dichloromethane (Table 2 and Figure 4). Addition of TFA to the dye solutions red-shifted the higher wavelength absorption because the charge-transfer transition and no changes were seen on the lower wavelength transitions. This shows that the TFA interacts with the dyes in such a way to alter the donor—acceptor interactions. Oxidation of the amine moiety may also influence the donor—acceptor interaction; however, it will lead to a blue shift in absorption. So it is concluded that the TFA supplies protons in the solution which shifts the equilibrium toward the acidic form. Addition of triethylamine to the toluene or dichloromethane solutions produced a drastic blue shift for the charge-transfer transition.

Adsorption of the dyes on transparent nanocrystalline anatase TiO$_2$ films shifts the absorption peak toward higher wavelength region (Figure 5) when compared to the corresponding spectra recorded for the dyes in dichloromethane. This is probably due to the use of thicker TiO$_2$ film.[15] On the contrary, dye—TiO$_2$

Table 2. Absorption Spectral Data for the Dyes in Different Solvents

| dye	TOL	TOL+TEA	TOL+TFA	MeOH	MeOH+NaOH	MeOH+TFA	DCM+TEA	DCM+TFA	ACN	THF
	λ_{max} nm (ε_{max}, $\times 10^3$ M^{-1} cm^{-1})									
D2	422 (22.2),	399 (27.6),	464 (28.7),	405 (32.5),	405 (32.8),	430 (34.3),	405 (28.1),	453 (36.7),	427 (30.2),	411 (20.3),
	326 (15.5)	340 (18.1)	320 (16.6)	324 (18.6),	324 (18.6),	317 (18.7),	331 (16.2)	319 (20.2),	318 (16.6)	433 (15.0)
				262 (22.1)	262 (23.0)	266 (20.8)		269 (20.5)		
JD1	446(33.9),	404 (36.9),	458 (36.2),	411 (36.5),	409 (40.6),	434 (22.9),	409 (35.8),	463 (32.5),	432 (29.0),	399 (36.0),
	367 (35.72)	366 (37.6)	367 (36.9)	360 (36.7)	360 (40.6)	360 (22.8)	365 (36.6),	364 (29.0),	359 (28.9)	364 (35.0)
							308 (23.0)	308 (21.7)		
JD2	440 (31.5),	388 (42.2)	456 (32.7),	407 (34.8),	405 (36.2),	430 (31.9),	385 (42.9),	457 (38.8),	417 (24.5),	382 (45.9),
	373 (36.3)		372 (36.5)	374 (38.3)	377 (39.8)	366 (33.6)	335 (26.7)	368 (28.8),	370 (30.0)	334 (27.6)
								269 (27.8)		
JD3	397 (23.4),	344 (34.8)	409 (22.9),	369 (26.5),	340 (38.4)	387 (30.0),	343 (48.9),	413 (38.8),	391 (15.2),	329 (41.2)
	326 (32.7)		330 (34.4)	327 (36.1)		323 (46.7)	294 (41.9),	329 (36.3),	324 (25.2)	
							284 (42.2)	291 (49.9)		
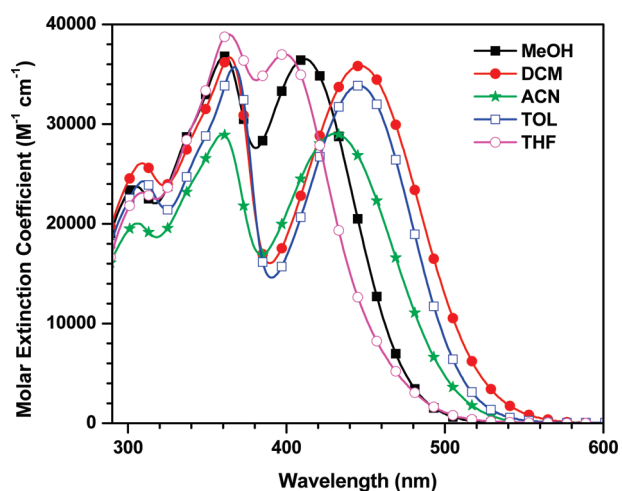
Figure 2. Absorption spectra of **JD1** recorded in different solvents.
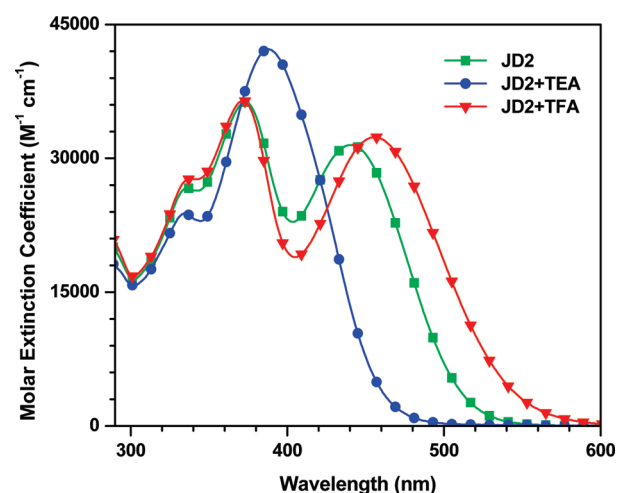

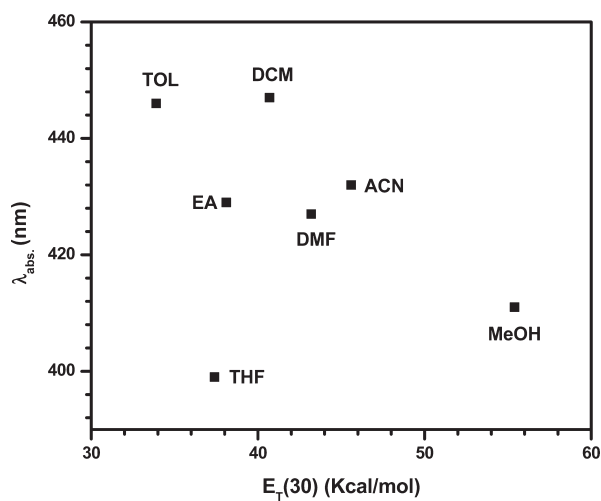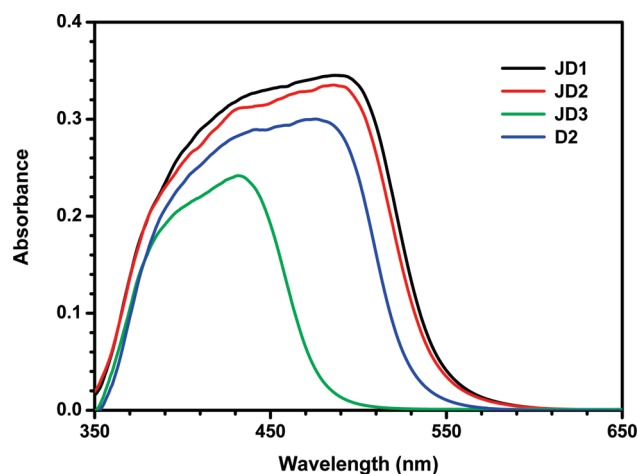**Figure 4.** Absorption spectra of the dye **JD2** recorded in toluene before and after the addition of TEA or TFA.


Figure 3. Variation of absorption peak positions observed for **JD1** in different solvents with $E_T(30)$ parameter.

Figure 5. Absorption spectra of the dyes anchored on nanocrystalline TiO$_2$.

Table 3. Computed Vertical Transition Energies and Their Oscillator Strengths and Configurations for the Dyes Using Different Theories

theory	parameter	D2	JD1	JD2	JD3
B3LYP (gas)	λ_{max}	446.5	519.8	501.4	421.0
	f	0.65	0.22	0.23	0.21
	configuration	HOMO→LUMO (100%)	HOMO→LUMO (100%)	HOMO→LUMO (99%)	HOMO→LUMO (95%)
CAM-B3LYP (gas)	λ_{max}	363.8	369.8	359.1	330.9
	f	0.95	1.02	1.10	1.10
	configuration	HOMO→LUMO (88%)	HOMO-1→LUMO (45%)	HOMO-1→LUMO (44%)	HOMO-1→LUMO (70%)
		HOMO-1→LUMO (6%)	HOMO→LUMO (43%)	HOMO→LUMO (40%)	HOMO→LUMO (17%)
			HOMO→LUMO+1 (5%)		
CAM-B3LYP (THF)	λ_{max}	382.1	385.3	372.2	347.4
	f	1.13	1.18	1.24	1.14
	configuration	HOMO→LUMO (93%)	HOMO→LUMO (53%)	HOMO→LUMO (61%)	HOMO-1→LUMO (68%)
			HOMO-1→LUMO (21%)	HOMO-1→LUMO (32%)	HOMO→LUMO (25%)
MPW1K (gas)	λ_{max}	373.1	387.2	372.0	336.0
	f	0.89	0.82	0.88	0.99
	configuration	HOMO→LUMO (94%)	HOMO→LUMO (68%)	HOMO→LUMO (65%)	HOMO-1→LUMO (69%)
			HOMO-1→LUMO (26%)	HOMO-1→LUMO (26%)	HOMO→LUMO (23%)
MPW1K (THF)	λ_{max}	391.4	404.5	387.3	352.4
	f	1.08	0.99	1.02	1.02
	configuration	HOMO→LUMO (93%)	HOMO→LUMO (63%)	HOMO→LUMO (61%)	HOMO-1→LUMO (68%)
			HOMO-1→LUMO (31%)	HOMO-1→LUMO (32%)	HOMO→LUMO (25%)
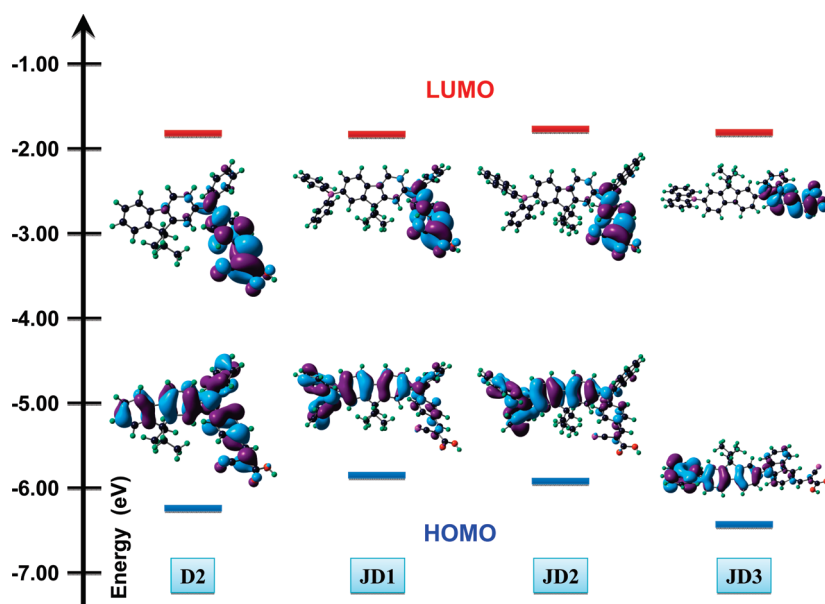
Figure 6. Energies and the electronic distribution of the frontier molecular orbitals of the dyes **JD1**−**JD3** and **D2** computed in THF using TDDFT/MPW1K/6-31G(D, P).

interactions or deprotonation of the dyes at the surface of the TiO$_2$ films would lead to a blue-shift.[2d]

To understand the electronic structure of the dyes, the geometry of the dyes was optimized by density functional theory[16] (DFT) calculations at the 6-31+G(D,P) level using three different correlation functionals (B3LYP,[17] CAM-B3LYP,[19] and MPW1K[19]), and the vertical excitation energies were computed using time-dependent density functional theory in the same level. The computed energies of the vertical excitations and their assignments are collected in Table 3. Figure 6 shows the electron distribution of the HOMO

and LUMO of the dyes along with their energies obtained using MPW1K. The HOMOs in the dyes are delocalized over the triarylamine unit constituted by the phenyl, naphthyl, or carbazole and fluorene segments with larger electron density located at the two nitrogen atoms of the amines, while the LUMOs are located in the cyanoacrylic acid unit through the phenyl group. Thus, the HOMO−LUMO excitation induced by light irradiation could move the electron distribution from the triarylamine part to the cyano-acrylic acid segment. This will ensure an efficient electron injection in the TiO$_2$ layer. The HOMO energies of the dyes increase in the
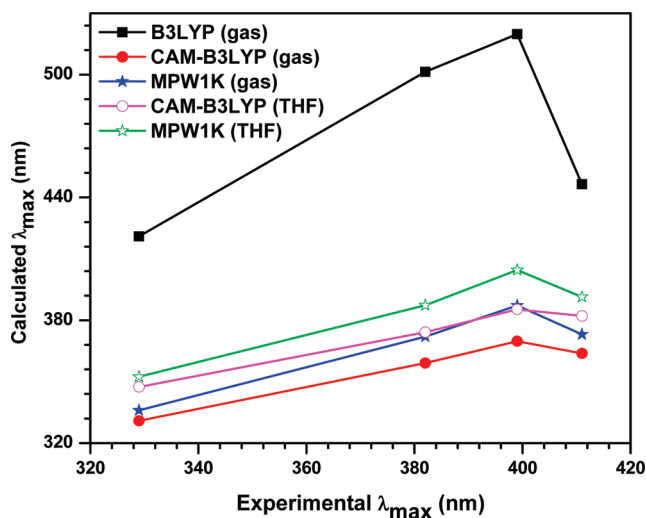
Figure 7. Comparison of observed (THF) and calculated electronic excitations for the dyes.

Figure 8. Cyclic voltammograms of the dyes **JD1**, **JD2**, and **D2** and their parent amines (**1a**, **1b**, and **1d**) recorded in dichloromethane solutions.

order, **JD1** < **JD2** < **D2** < **JD3**, while the LUMO energies remain unaltered. It has been suggested in a recent work that the HOMO energies have to match the redox potential of the redox electrolyte to achieve effective regeneration of the dyes in DSSC. It appears that by altering the donor strength of the additional donor groups in a D-π-D-π-A architecture, the HOMO levels can be adjusted while retaining the LUMO levels.

The vertical excitations, corresponding to the HOMO to LUMO transitions obtained for the dyes in different theory levels, are plotted against the experimental absorption maxima observed in THF in Figure 7. The longer wavelength transition calculated using B3LYP for the dyes are red-shifted from the observed values in tetrahydrofuran, whereas the gas phase results obtained from CAM-B3LYP and MPW1K methods are showing slight blue shift (Table 3). However, the vertical excitations calculated in the presence of tetrahydrofuran using PCM and CAM-B3LYP or MPW1K show close agreement to the experimentally observed values for tetrahydrofuran. Though the higher wavelength absorption in the dyes is predicted to originate from the HOMO/LUMO transition in B3LYP calculations, CAM-B3LYP and MPW1K results suggested contributions from HOMO/LUMO and HOMO-1/LUMO transitions for the dyes **JD1**−**JD3**. On this basis, it may be argued that the longer wavelength absorption present in these dyes possesses a contribution from the π−π^* transition as well.

Electrochemical Properties. Cyclic voltammetry measurements on the dyes were performed to determine the oxidation potentials (E_{ox}) of the dyes and the excited-state oxidation potential (E_{ox}^*). The later quantity can be obtained by subtracting the 0−0 transition energy (E_{0-0}) from E_{ox}, whereas E_{0-0} is derived from the absorption edge of the dye.[20] The data obtained from the electrochemical measurements are listed in Table 1.

The dyes **JD1** and **JD2** displayed two quasi-reversible oxidation couples (Figure 8), excluding the redox couple arising due to the internal ferrocene standard. The first oxidation occurring at ca. 250 mV corresponds to the removal of electron from the amine furthest away from the electron-withdrawing segment. The second oxidation occurs at more positive potentials (>520 mV) and originates from the removal of an electron from the amino segment in direct conjugation with the cyanoacrylic acid unit. This amine unit is difficult to oxidize when compared to the peripheral amine as
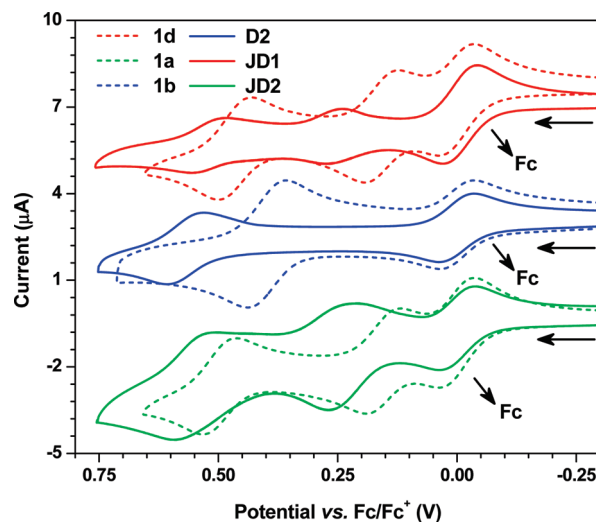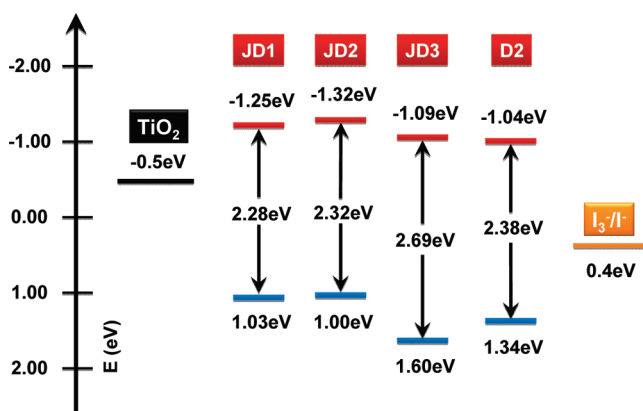

Figure 9. Comparison of the oxidation potentials of the dyes **JD1**−**JD3** and **D2** dissolved in dichloromethane in the ground and excited states.

the electron density on the nitrogen is depleted by the electron-accepting cyanoacrylic unit. The oxidation potential observed for the control dye **D2** is close to the second oxidation potential observed for the dyes **JD1** and **JD2**. This also confirms the assignment. The first oxidation potentials of the dyes (**JD1**, **JD2**, and **D2**) are positively shifted when compared to the parent amines **1a**, **1b**, and **1d** (Figure 8), which confirms the electron-withdrawing effect of the acceptor segment. Similarly, there is a slight negative shift for the second oxidation potentials of the dyes when compared to the oxidation potential of the control dye **D2**, which reflects the electron-donating effect of the additional amine unit on facilitating the oxidation of the amine adjacent to the acceptor unit.

The variation of oxidation potentials in the ground and excited states for the dyes are illustrated in Figure 9. For comparison, the conduction band of TiO$_2$ layer and the redox potential of the redox electrolyte (I$^-$/I$_3^-$) used in the DSSC is also included.[21] The incorporation of additional diarylamine segment in the dye structure is beneficial to raise both the E_{ox} and E_{ox}^* but narrows the band gap. Stronger donors obviously result in larger donor−acceptor interaction, which leads to the reduction in the E_{0-0}. The ground-state oxidation potentials of the dyes occupy a wide range covering 1.03 to 1.60 V versus NHE and are more positive

Table 4. Performance Parameters of the DSSCs Fabricated Using the Dyes JD1−3 and D2

dye	J_{SC} (mA cm^{-2})	V_{OC} (mV)	ff	η (%)	R_{Ct2} (Ω)	τ_e (ms)
JD1	10.4	571	0.69	4.11	17.30	15.27
JD2	10.5	595	0.70	4.36	15.36	22.69
JD3	5.46	605	0.70	2.30	28.79	27.68
D2	8.73	603	0.69	3.60	19.28	22.69
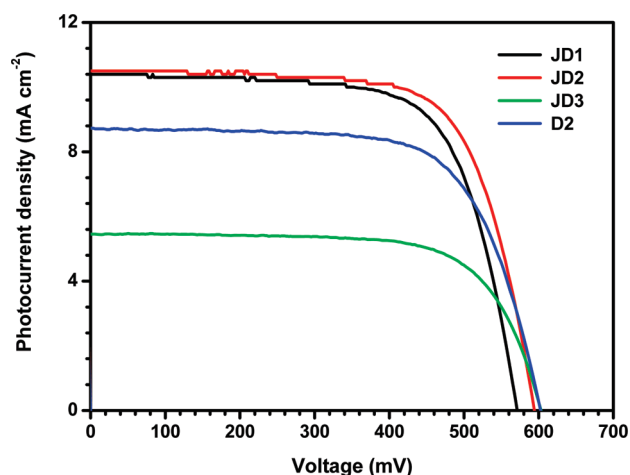
Figure 10. I−V characteristics of the DSSCs fabricated using the dyes JD1−JD3 and D2.

Figure 11. IPCE plots of the DSSCs fabricated using the dyes JD1−JD3 and D2.

Figure 12. Equivalent circuit for the DSSCs.

than the redox potential of iodine/iodide couple.[21] The excited state oxidation potentials of the dyes are in between −1.04 and −1.32 V versus NHE and more negative than the conduction band of TiO$_2$, which is located at ca. −0.5 V versus NHE.[22] These observations indicate that the redox potentials of the dyes in the ground and excited states are favorable for efficient electron injection to TiO$_2$ and the dye regeneration by iodine/iodide redox system.

DSSC Characteristics. The photovoltaic performances (Table 4) of the newly synthesized dyes (**D2, JD1−JD3**) were evaluated using the Grätzel photoelectrochemical cells. Figure 10 shows I−V characteristics, while Figure 11 displays the IPCE action spectra for DSSCs based on these four dyes using a 18.5 μm TiO$_2$ (14 μm transparent layer +4.5 μm scattering layer) electrode. IPCE is defined as the number of electrons generated by light in the external circuit divided by the number of incident photons. The dyes exhibit maximum IPCE (>75%) between 400 and 500 nm and the IPCE spectra broadens and extends to 600 nm on incorporation of additional diarylamine unit (for example, compare **D2** with **JD1** or **JD2**) which is consistent with the bathochromic shift observed for these dyes in the UV−vis absorption spectra of the dye loaded TiO$_2$ films (Figure 5). The broadening of the IPCE spectra is desired for a larger photocurrent[23] which explains the higher efficiency observed for the dyes **D2, JD1**, and **JD2** when compared to the carbazole dye **JD3**. J_{SC} increased in the order of **JD3 < D2 < JD1 < JD2** as a result of the broadening of the IPCE spectra and is similar to the trend observed for the absorption peak in dichloromethane solution.[24] DSSC based on **JD1** showed lower V_{OC} when compared to the DSSCs fabricated using the other dyes (**JD2, JD3,** and **D2**). In general, the lower V_{OC} of a DSSC is attributed to the shorter electron lifetime, τ_e.[25]

There are four critical processes that determine the photovoltaic performance of the DSSC: electron injection from the dye
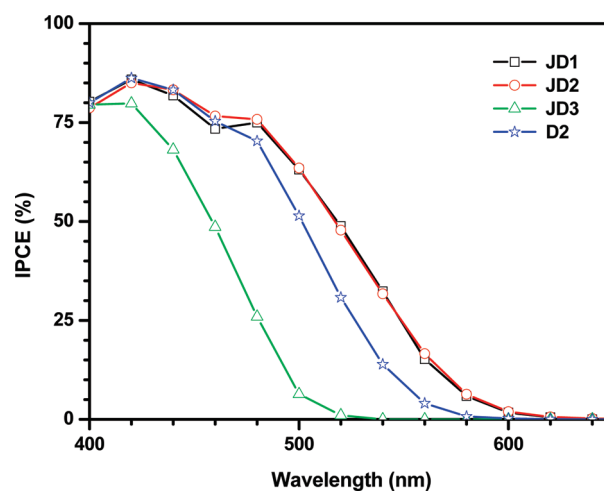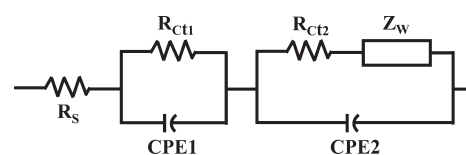
to the conduction band of TiO$_2$; recombination of the injected electrons on TiO$_2$ with the oxidized dye; dark current generated due to the reduction of I$_3^-$ by the injected electrons; and the regeneration of the dye by the electrolyte which is dependent on the HOMO level of the dye and the redox potential of the electrolyte. As the electron injection and regeneration of the dye are largely dependent on the electronic properties of the dyes, we will first examine the electron injection propensity and the regeneration feasibility for the dyes. For a facile electron injection, the excited-state oxidation potential of the dyes must be more negative than that of the TiO$_2$ conduction band. The excited state oxidation potentials of the dyes assume the following order: **JD2 < JD1 < JD3 < D2**. More negative excited state oxidation potential observed for **JD2** among the series gives larger driving force the electron injection from this dye. However, this trend is not matching with the photovoltaic efficiency trend which indicates that other factors also influence the photovoltaic performance. The HOMO energies of the dyes deduced in dichloromethane solution are in the order, **JD2 > JD1 > D2 > JD3**. This suggests that the regeneration will be more facile for **JD2** when compared to the other dyes.

The effects of the different dyes on the electron transport at the interfaces in the DSSCs can be estimated with the aid of electrochemical impedance spectroscopy (EIS) measurements. The electrochemical impedance analysis of the DSSCs were performed over the frequency range of 10 mHz to 65 kHz under illumination at the applied bias voltage set at the open-circuit voltage of the DSSCs with an ac amplitude of 10 mV. In general, the EIS spectrum of a dye-sensitized solar cell having a configuration FTO/TiO$_2$/dye/electrolyte/Pt/ITO displays three semicircles in the frequency range of 10 mHz to 65 kHz. The equivalent circuit is shown in Figure 12. The ohmic serial resistance (R_S) corresponds to the overall series resistance. The first and second semicircles
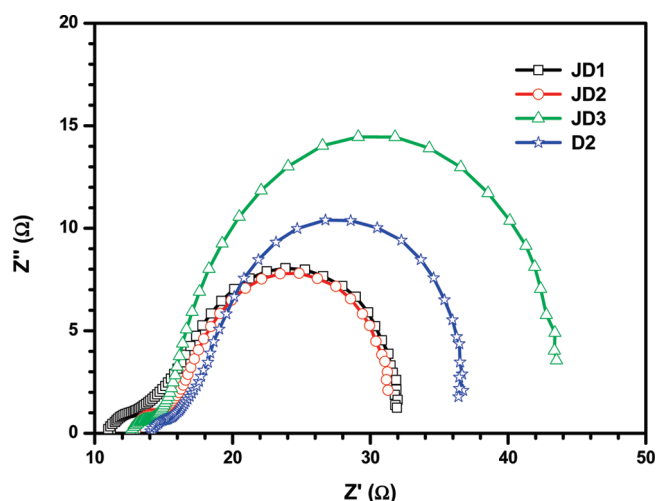
Figure 13. Nyquist plots of the DSSCs fabricated using the dyes **JD1**−**JD3** and **D2**.
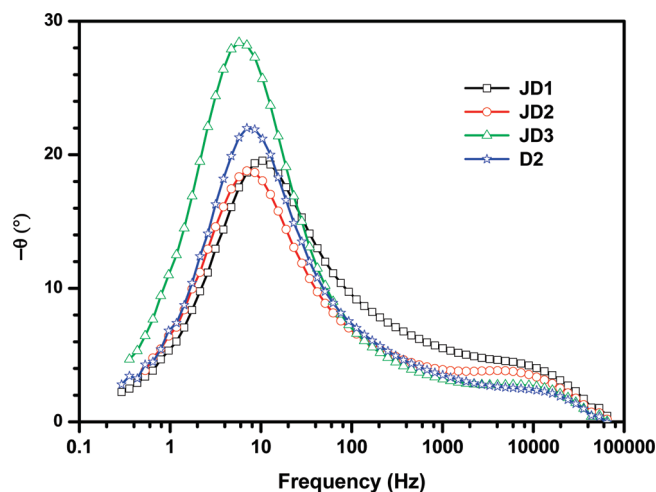

Figure 14. Bode-phase plots of the DSSCs fabricated using the dyes **JD1**−**JD3** and **D2**.

correspond to the charge-transfer resistances at the counter electrode (R_{ct1}) and the TiO$_2$/dye/electrolyte interface (R_{ct2}), respectively. The Warburg diffusion process of I$^-$/I$_3^-$ in the electrolyte (Z_w) is associated with the third semicircle. However, in this work the conventional diffusion resistance of the redox couple is apparently greatly overlapped by R_{ct2} because of a short length for I$^-$ ion diffusion available with the thin spacer used (25 μm thick) and owing to the low viscosity of the solvents used in our electrolyte (viscosities of ACN and MPN are 0.37 and 1.60 cP, respectively). The Nyquist plot displayed in Figure 13 shows two semicircles which correspond to the charge-transfer resistances at the counter electrode and TiO$_2$/dye/electrolyte interface, respectively. The radius of the bigger semicircle of the dye **JD3** is significantly larger than the other dyes, indicating the enlarged charge-transfer resistance for this dye. The charge-transfer resistance assumes the order **JD2** < **JD1** < **D2** < **JD3**. Though the charge-transfer resistance of **JD2** is smaller than that of **JD1**, the V_{oc} is larger. The larger V_{oc} observed for **JD2** may originate from the enhanced electronic coupling between the amino segment of the

dye and the electrolyte constituents. The presence of naphthyl group in **JD2** may facilitate the electronic coupling when compared to the phenyl unit in **JD1**.

In the Bode phase plot (Figure 14) the lower frequency peak of the dye **JD1** is shifted to higher frequency when compared to those of other dyes. This corresponds to a decrease in the electron lifetime for the **JD1** sensitized DSSC. The electron lifetime can be extracted from the angular frequency (ω_{min}) at the midfrequency peak in the Bode phase plot using $\tau_e = 1/\omega_{min}$.[26] The electron lifetime follows the trend, **JD1** < **JD2** ∼ **D2** < **JD3**. The increase in electron lifetime supports more effective suppression of the back reaction of the injected electrons with the I$_3^-$ in the electrolyte by alternation of HOMO of the sensitizer, which leads to the improvement in the photocurrent and photovoltage and to the substantial enhancement of the device efficiency for the dye **JD2**. Despite the enhancement in the electron lifetime, the lower device efficiency observed for the DSSC based on **JD3** is attributed to the lower number of photoinduced electron generation and lesser electron injection efficiency of **JD3**. The high-frequency peak observed in the Bode plot corresponds to charge transfer at the counter electrode. Slight changes observed for this peak indicate a probable reaction at the counter electrode/electrolyte interface.

CONCLUSIONS

In summary, we have synthesized four new dyes based on triarylamine donors featuring additional diarylaminofluorene chromophores and cyanoacrylic acid acceptors. They were characterized by optical and electrochemical studies. They display red-shifted absorption and negatively shifted oxidation potentials when compared to the simple triphenylamine-based dyes. Subsequently, they exhibit improved light-harvesting performance in nanocrystalline anatase TiO$_2$-based dye-sensitized solar cells when compared to the parent dyes derived from the monoamines. The enhanced light-to-electron conversion efficiency is attributed to the broader and intense absorption profile observed for the fluorenediamine-based dyes and their high lying HOMO. The enhanced optical property contributes to the increase in the photocurrent density and the comparatively larger HOMO value facilitates the regeneration of the dyes by the electrolyte and suppression of the back reaction of the injected electrons with the electrolyte constituents. The success of the design strategy used in this work to improve the device performance indicates that the fluoreneamine additional donors may be incorporated in the demonstrated dye architectures to obtain efficient organic dyes for dye-sensitized solar cells.

EXPERIMENTAL SECTION

General Methods. All reactions and manipulations were carried out under N$_2$ with the use of standard inert atmosphere and Schlenk techniques. Solvents were dried by standard procedures. All column chromatography was performed with the use of 100−200 mesh silica gel as the stationary phase in a column of 30 cm long and 2.0 cm diameter. The ^{1}H and ^{13}C NMR spectra were measured by using 500 MHz spectrometer. Cyclic voltammetric experiments were carried out at room temperature with a conventional three-electrode configuration consisting of a glassy carbon working electrode, a platinum wire auxiliary electrode, and a nonaqueous Ag/AgNO$_3$ reference electrode. The $E_{1/2}$ values were determined as $^1/_2(E_p^a + E_p^c)$, where E_p^a and E_p^c are the anodic and cathodic peak potentials, respectively. The potentials are quoted against the ferrocene internal standard. The solvent in all experiments was dichloromethane and the supporting electrolyte was 0.1 M tetrabutylammonium perchlorate. Electronic absorption spectra

were obtained on a UV–visible spectrophotometer using freshly prepared solutions. The precursor compounds **1a–d** were obtained according to the literature procedures.[27–29]

4-((9,9-Diethyl-9H-fluoren-2-yl)(phenyl)amino)benzaldehyde (2a): yellow solid; yield 60%; mp 86 °C; IR (KBr, cm^{-1}) 1676 ($\nu_{C=O}$); ^{1}H NMR (CDCl$_3$, 500.13 MHz) δ 0.34–0.37 (m, 6 H), 1.91–2.17 (m, 4 H), 7.07 (d, J = 8.5 Hz, 2 H), 7.11 (dd, J = 8.0, 2.0 Hz, 1 H), 7.15–7.22 (m, 4 H), 7.30–7.36 (m, 4 H), 7.65–7.71 (m, 4 H), 9.82 (s, 1 H); ^{13}C NMR (CDCl$_3$, 125.75 MHz) δ 190.5, 153.5, 151.8, 150.1, 146.4, 145.3, 140.8, 138.9, 131.4, 129.8, 129.7, 128.1, 125.0, 122.9, 121.3, 120.8, 119.7, 119.6, 119.4, 56.2, 32.7, 8.6.

4-((7-(Diphenylamino)-9,9-diethyl-9H-fluoren-2-yl)(phenyl)amino)benzaldehyde (2b). A two-neck flask was charged with 9,9-diethyl-N^2,N^2,N^7,N^7-tetraphenyl-9H-fluorene-2,7-diamine (3.33 g, 6.0 mmol). This was dissolved in 15 mL of chlorobenzene and 10 mL of DMF with stirring. POCl$_3$ (0.6 mL, 6.6 mmol) was then added dropwise into the mixture at room temperature. The mixture was heated at 90 °C for 10 h with stirring. It was then poured into ice–water and neutralized with sodium bicarbonate. The organic products formed were extracted with dichloromethane (3 × 50 mL). The combined organic extracts were concentrated and adsorbed on silica gel and purified by column chromatography by using hexane/ethyl acetate mixture (5:1) as eluant: yellow solid; yield 2.27 g (65%); mp 170 °C; IR (KBr, cm^{-1}) 1685 ($\nu_{C=O}$); ^{1}H NMR (CDCl$_3$, 500.13 MHz) δ 0.39–0.42 (m, 6 H), 1.84–1.88 (m, 4 H), 7.01–7.10 (m, 7 H), 7.13–7.15 (m, 5 H), 7.15–7.18 (m, 1 H), 7.22 (d, J = 7.5 Hz, 2 H), 7.26–7.29 (m, 4 H), 7.35–7.38 (m, 2 H), 7.54 (d, J = 8.5 Hz, 1 H), 7.58 (d, J = 8.0 Hz, 1 H), 7.71 (d, J = 9.0 Hz, 2 H), 9.83 (s, 1 H); ^{13}C NMR (CDCl$_3$, 125.75 MHz) δ 190.4, 153.5, 151.7, 151.4, 147.9, 147.1, 146.3, 144.5, 138.7, 135.8, 131.3, 129.6, 129.2, 128.9, 125.8, 125.5, 124.8, 123.9, 123.6, 122.5, 121.2, 120.2, 120.1, 119.3, 119.2, 56.1, 32.5, 8.6; HRMS calcd for C$_{42}$H$_{37}$N$_2$O [M + H] m/z 585.2906, found 585.2918.

4-((9,9-Diethyl-7-(naphthalen-1-yl(phenyl)amino)-9H-fluoren-2-yl)(naphthalen-1-yl)amino)benzaldehyde. (2c). A two-neck flask was charged with 9,9-diethyl-N^2,N^7-di(naphthalen-1-yl)-N^2,N^7-diphenyl-9H-fluorene-2,7-diamine (1.0 g, 1.52 mmol). This was dissolved in chlorobenzene (5 mL) and N-methylformanilide (0.35 mL). POCl$_3$ (0.35 mL, 3.85 mmol) was then added to slowly at room temperature. The resultant mixture was allowed to heat at 90 °C for 15 h and then poured into ice–water and neutralized with sodium bicarbonate. The organic products formed were extracted with dichloromethane (3 × 50 mL). The combined organic extracts were concentrated and adsorbed on silica gel. It was purified by column chromatography by using hexane/ethyl acetate mixture (5:1) as eluant: yellow solid; yield 0.46 g (44%); mp 175 °C; IR (KBr, cm^{-1}): 1685 ($\nu_{C=O}$); ^{1}H NMR (CDCl$_3$, 500.13 MHz) δ 0.32 (t, J = 7.5 Hz, 6H), 6.88–6.94 (m, 4H), 7.02–7.07 (m, 4H), 7.18–7.22 (m, 3H), 7.31–7.33 (m, 2H), 7.38–7.51 (m, 8H), 7.64 (d, J = 9.0 Hz, 2H), 7.75 (d, J = 8.5 Hz, 1H), 7.83 (d, J = 8.0 Hz, 1H), 7.86–7.92 (m, 4H), 9.77 (s, 1H); ^{13}C NMR (CDCl$_3$, 125.75 MHz) δ 190.4, 154.2, 151.4, 151.3, 148.8, 144.6, 143.9, 142.1, 138.5, 135.3, 134.9, 131.3, 130.9, 130.6, 129.1, 128.6, 128.4, 127.51, 127.1, 126.7, 126.7, 126.4, 126.3, 126.3, 126.2, 126.6, 126.7, 124.2, 124.1, 123.8, 121.8, 121.60, 121.4, 120.0, 119.9, 119.6, 117.7, 116.9, 56.1, 32.5, 8.4; HRMS calcd for C$_{50}$H$_{41}$N$_2$O [M + H] m/z 685.3219, found 685.3242.

9-(7-(9H-Carbazol-9-yl)-9,9-diethyl-9H-fluoren-2-yl)-9H-carbazole-3-carbaldehyde. (2d). In a round-bottom flask, 9,9'-(9,9-diethyl-9H-fluorene-2,7-diyl)bis(9H-carbazole) (1.0 g, 1.81 mmol) was dissolved in chlorobenzene (5 mL) and N,N-dimethylformamide (3 mL) under nitrogen atmosphere. In a separate reaction flask, POCl$_3$ (0.40 mL, 4.0 mmol) was added slowly to DMF (2 mL) at 0 °C under nitrogen atmosphere and the mixture kept at room temperature for 1 h. This Vilsmeier reagent was then added to the reaction mixture. The resultant mixture was allowed to heat at 100 °C for 15 h and then poured into ice–water and neutralized with sodium bicarbonate. The organic products formed were extracted with dichloromethane (3 × 50 mL). The combined

organic extracts were concentrated and adsorbed on silica gel. It was purified by column chromatography by using hexane/ethyl acetate mixture (5:1) as eluant: cream-white solid; yield 0.27 g (30%); mp 233 °C; IR (KBr, cm^{-1}) 1686 ($\nu_{C=O}$); ^{1}H NMR (CDCl$_3$, 500.13 MHz) δ 0.55–0.58 (m, 6 H), 2.10–2.14 (dd, J = 15 Hz, 7.5 Hz, 4 H), 7.31–7.34 (m, 2 H), 7.40–7.64 (m, 12 H), 7.99–8.04 (m, 3 H), 8.19 (d, J = 7.5 Hz, 2 H), 8.25 (d, J = 8.0 Hz, 1 H), 8.71 (d, J = 1.0 Hz, 1 H); ^{13}C NMR (CDCl$_3$, 125.75 MHz) δ 191.7, 152.4, 152.1, 144.6, 142.0, 141.0, 140.9, 139.6, 137.1, 135.6, 129.5, 127.6, 127.1, 126.2, 126.0, 123.9, 123.6, 123.4, 123.3, 121.9, 121.2, 121.2, 121.2, 120.8, 120.4, 120.0, 110.4, 110.1, 109.7, 56.8, 32.7, 8.8; HRMS calcd for C$_{42}$H$_{32}$N$_2$O m/z 580.2515, found 580.2527.

(E)-2-Cyano-3-(4-((7-(diphenylamino)-9,9-diethyl-9H-fluoren-2-yl)(phenyl)amino)phenyl)acrylic Acid (JD1). A mixture of the aldehyde **2b** (1.0 g, 1.71 mmol), 2-cyanoacetic acid (0.18 g, 1.90 mmol), ammonium acetate (0.58 g, 0.75 mmol), and acetic acid (5 mL) was refluxed for 12 h. The resulting dark red solution was poured into water. The separated solid was filtered and thoroughly washed with water and dried: orange powder; yield 0.90 g (80%); mp 190 °C; IR (KBr, cm^{-1}) 2216 ($\nu_{C\equiv N}$); ^{1}H NMR (DMSO-d$_6$, 500.13 MHz) δ 0.26–0.29 (m, 6 H), 1.79–1.84 (m, 4 H), 6.89 (d, J = 9.0 Hz, 2 H), 6.93–6.95 (dd, J = 8.5 Hz, 2.0 Hz, 1 H), 7.00–7.02 (m, 6 H), 7.06 (d, J = 1.5 Hz, 1 H), 7.11–7.13 (dd, J = 8.5 Hz, 2.0 Hz, 1 H), 7.20–7.30 (m, 8 H), 7.39–7.43 (m, 2 H), 7.69 (d, J = 8.0 Hz, 1 H), 7.74 (d, J = 8.0 Hz, 1 H), 7.91 (d, J = 9.0 Hz, 2 H), 8.11 (s, 1 H); ^{13}C NMR (DMSO-d$_6$, 125.75 MHz) δ 164.6 152.9, 151.3, 148.60, 147.8, 144.1, 143.5, 141.5, 138.5, 135.4, 135.3, 134.9, 133.3, 130.7, 130.4, 129.7, 129.2, 129.03, 128.6, 128.2, 127.6, 127.4, 127.1, 127.0, 126.9, 126.8, 126.2, 124.7, 124.0, 123.5, 122.9, 122.1, 121.7, 121.5, 121.0, 120.7, 120.4, 117.3, 117.8, 116.4, 56.1, 32.1, 8.9; HRMS calcd for C$_{45}$H$_{38}$N$_3$O$_2$ [M + H] m/z 652.2959, found 652.2961. Anal. Calcd for C$_{45}$H$_{37}$N$_3$O$_2$: C, 82.92; H, 5.72; N, 6.45. Found: C, 82.81; H, 5.64; N, 6.53.

(E)-2-Cyano-3-(4-((9,9-diethyl-7-(naphthalen-1-yl(phenyl)amino)-9H-fluoren-2-yl)(naphthalen-1-yl)amino)phenyl)acrylic Acid (JD2). Compound **JD2** was prepared in 86% yield from **2c** by following a procedure similar to that described above for **JD1**: dark red solid; mp 202 °C; IR (KBr, cm^{-1}) 2218 ($\nu_{C\equiv N}$); ^{1}H NMR (DMSO-d$_6$, 500.13 MHz) δ 0.21 (t, J = 7.5 Hz, 6 H), 1.65–1.80 (m, 4 H), 6.72 (d, J = 8.5 Hz, 2 H), 6.80–6.82 (m, 1 H), 6.90-6.98 (m, 4 H), 7.10–7.12 (m, 1 H), 7.22 (t, J = 8.0 Hz, 2 H), 7.32–7.37 (m, 3 H), 7.46–7.48 (m, 2 H), 7.52–7.57 (m, 4 H), 7.53–7.57 (m, 3 H), 7.81–7.88 (m, 5 H), 7.96–8.05 (m, 4 H); ^{13}C NMR (DMSO-d$_6$, 125.75 MHz) δ 164.6 152.9, 151.3, 148.60, 147.8, 144.1, 143.5, 141.5, 138.5, 135.4, 135.3, 134.9, 133.3, 130.7, 130.4, 129.7, 129.2, 129.03, 128.6, 128.2, 127.6, 127.4, 127.1, 127.0, 126.9, 126.8, 126.2, 124.7, 124.0, 123.5, 122.9, 122.1, 121.7, 121.5, 121.0, 120.7, 120.4, 117.3, 117.8, 116.4, 56.1, 32.1, 8.9; HRMS calcd for C$_{53}$H$_{42}$N$_3$O$_2$ [M + H] m/z 752.3273, found 752.3273. Anal. Calcd for C$_{53}$H$_{41}$N$_3$O$_2$: C, 84.66; H, 5.50; N, 5.59. Found: C, 84.78; H, 5.61; N, 5.47.

(E)-3-(9-(7-(9H-Carbazol-9-yl)-9,9-diethyl-9H-fluoren-2-yl)-9H-carbazol-3-yl)-2-cyanoacrylic Acid (JD3). Compound **JD3** was obtained in 82% yield from **2d** by following the general procedure described for **JD1**: yellow solid; mp 282 °C; IR (KBr, cm^{-1}) 2221 ($\nu_{C\equiv N}$); ^{1}H NMR (DMSO-d$_6$, 500.13 MHz) δ 0.45 (t, J = 7.5 Hz, 1H), 2.16–2.20 (m, 4H), 7.32 (t, J = 7.5 Hz, 2 H), 7.45–7.40 (m, 4 H), 7.49 (t, J = 7.5 Hz, 2 H), 7.53 (d, J = 8.5 Hz, 1 H), 7.58 (t, J = 7.5 Hz, 1 H), 7.71–7.65 (m, 2 H), 7.84–7.78 (m, 2 H), 8.51–8.25 (m, 6 H), 9.00 (s, 1 H); ^{13}C NMR (DMSO-d$_6$, 125.75 MHz) δ 164.4, 152.5, 152.4, 143.3, 141.8, 140.8, 136.7, 135.4, 128.8, 126.8, 126.5, 124.0, 123.2, 122.8, 122.2, 121.9, 121.0, 120.5, 110.0, 57.1, 32.0, 9.1; HRMS calcd for C$_{45}$H$_{34}$N$_3$O$_2$ [M + H] m/z 648.2646, found 648.2648. Anal. Calcd for C$_{45}$H$_{33}$N$_3$O$_2$: C, 83.44; H, 5.13; N, 6.49. Found: C, 83.32; H, 5.07; N, 6.45.

(E)-2-Cyano-3-(4-((9,9-diethyl-9H-fluoren-2-yl)(phenyl)amino)phenyl)acrylic Acid (D2). Compound **D2** was obtained in 64% yield from **2a** by following the general procedure described for

JD1: red solid; IR (KBr, cm^{-1}) 2219 ($\nu_{C\equiv N}$); ^{1}H NMR (CDCl$_3$, 500.13 MHz) δ 0.24 (t, J = 7.5 Hz, 6 H), 1.90−1.97 (m, 4 H), 6.89−6.92 (m, 2 H), 7.14−7.23 (m, 1 H), 7.24−7.31 (m, 7 H), 7.33−7.35 (m, 3 H), 7.41−7.44 (m, 3 H), 7.78−7.80 (m, 1 H), 7.85 (d, J = 8.0 Hz, 1 H), 7.92 (d, J = 9.0 Hz, 2 H), 8.13 (s, 1 H); ^{13}C NMR (DMSO-d_6, 125.75 MHz) δ 164.6, 153.7, 152.3, 151.8, 151.5, 150.1, 145.8, 145.4, 144.9, 140.7, 140.0, 139.2, 138.0, 133.4, 130.4, 127.7, 127.6, 126.5, 126.3, 126.2, 125.9, 123.4, 123.3, 122.0, 121.7, 120.9, 120.2, 118.9, 118.7, 117.5, 56.2, 32.2, 8.9; HRMS calcd for C$_{33}$H$_{29}$N$_2$O$_2$ [M + H] m/z 485.2225, found 485.2226. Anal. Calcd for C$_{33}$H$_{28}$N$_2$O$_2$: C, 81.79; H, 5.82; N, 5.78. Found: C, 81.92; H, 5.73; N, 5.71.

Computational Methods. All the computations were performed with the Gaussian 09 program package.[30] The ground-state geometries were fully optimized without any symmetry constrains at the DFT level with Becke's[31] three-parameter hybrid functional and Lee, Yang, and Parr's correlational functional B3LYP[17] using the 6-31g(d,p) basis set on all atoms. Vibrational analysis on the optimized structures was performed to confirm the structure. The excitation energies and oscillator strengths for the lowest 10 singlet−singlet transitions at the optimized geometry in the ground state were obtained by TD-DFT calculations using the same basis set as for the ground state and three kinds of hybrid functional B3LYP, CAM-B3LYP,[18] and MPW1K,[19] respectively. Solvation effects were modeled using the polarizable continuum model (PCM)[32] implemented in the Gaussian program, for both geometry optimizations and TD-DFT calculations.

DSSC Fabrication and Characterization. For the TiO$_2$ colloid solution, the TiO$_2$ precursor was prepared by the sol−gel method as described below. Titanium(IV) tetraisopropoxide (72 mL) was added to 430 mL of a 0.1 M nitric acid aqueous solution with constant stirring and heated to 85 °C simultaneously for 8 h. When the mixture was cooled to room temperature, the resultant colloid was transferred to an autoclave and then heated at 240 °C for 12 h in order to allow the TiO$_2$ particles to grow uniformly (ca. 20 nm). Consequently, the TiO$_2$ colloid was concentrated to 10 wt % (with respect to the TiO$_2$). The first type of TiO$_2$ paste (for transparent layer) was prepared by the addition 25 wt % (with respect to the TiO$_2$) of poly(ethylene glycol) (PEG, MW ∼20000) to the above solution in order to control the pore diameters and to prevent the film from cracking during drying. For the second one (for scattering layer), the first type of TiO$_2$ paste was incorporated with 50 wt % of light scattering TiO$_2$ particles for reducing the light loss by back scattering.

A fluorine-doped SnO$_2$ conducting glass (FTO, 7 Ω sq^{-1}, transmittance ∼80%) was first cleaned with a neutral cleaner and then washed with deionized water, acetone, and isopropyl alcohol, sequentially. The conducting surface of the FTO was treated with a solution of titanium tetraisopropoxide (1 g) in 2-methoxyethanol (3 g) to obtain a good mechanical contact between the conducting glass and TiO$_2$ film, as well as to isolate the conducting glass surface from the electrolyte. TiO$_2$ pastes were coated onto the treated conducting glass by using the doctor blade technique. To coat each TiO$_2$ layer, the dried TiO$_2$ film was gradually heated to 450 °C in an oxygen atmosphere and subsequently sintered at that temperature for 30 min. The TiO$_2$ photoanodes of the DSSCs employed in the experiments were composed of a 14 μm thick transparent TiO$_2$ layer and with a scattering layer of 4.5 μm thickness. After sintering at 450 °C and cooling to 80 °C, the TiO$_2$ film was immersed in a 3 × 10^{-4} M solution of dye at room temperature for 24 h. The standard ruthenium complex, N719, was dissolved in acetonitrile (ACN) and *tert*-butyl alcohol (volume ratio of 1:1) to make a reference dye solution. Various organic dye solutions were prepared in a mixing solvent containing ACN, *tert*-butyl alcohol, and dimethyl sulfoxide (DMSO) (volume ratio of 1:1:3). The thus prepared TiO$_2$/dye electrode was placed on a platinum-sputtered conducting glass electrode (ITO, 7 Ω sq^{-1}), keeping the two electrodes separated by a 25 μm thick Surlyn. The two electrodes were then sealed by heating. A mixture of

0.1 M LiI, 0.6 M DMPII, 0.05 M I$_2$, and 0.5 M TBP in 3-methoxypropionitrile (MPN)/ACN (volume ratio of 1:1) was used as the electrolyte. The electrolyte was injected into the gap between the electrodes by capillarity; the electrolyte-injecting hole was previously made in the counter electrode with a drilling machine, and the hole was sealed with hot-melt glue after the injection of the electrolyte.

The surface of the DSSC was covered by a mask with a light-illuminated area of 0.16 cm^2 and then illuminated by a class A quality solar simulator. Incident light intensity (100 mW cm^{-2}) was calibrated with a standard silicon cell. Photocurrent−voltage curves of the DSSCs were obtained with a potentiostat/galvanostat. The thickness of the TiO$_2$ film was judged by scanning electron microscopic images (SEM). For UV absorption spectra, dye molecules were coated on the TiO$_2$ films, and the corresponding spectra were obtained using an UV−vis spectrophotometer equipped with an integrating sphere. Electrochemical impedance spectra (EIS) were obtained from the potentiostat/galvanostat, equipped with an FRA2 module, under a constant light illumination of 100 mW cm^{-2}. The frequency range explored was 10 mHz to 65 kHz. The applied bias voltage was set at the open-circuit voltage of the DSSC between the ITO−Pt counter electrode and the FTO−TiO$_2$ dye working electrode, starting from the short-circuit condition; the corresponding AC amplitude was 10 mV. The impedance spectra were analyzed using an equivalent circuit model. Incident phototo-current conversion efficiency (IPCE) curves were obtained under short-circuit conditions. The light source was a class A quality solar simulator (PEC-L11, AM 1.5 G); light was focused through a monochromator onto the photovoltaic cell. The monochromator was incremented through the visible spectrum to generate the IPCE (λ) as defined by IPCE (λ) = 1240 ($J_{SC}/\lambda\varphi$), where λ is the wavelength, J_{SC} is the short-circuit photocurrent density (mA cm^{-2}) recorded with a potentiostat/galvanostat, and φ is the incident radiative flux (W m^{-2}) measured with an optical detector and a power meter.

■ ASSOCIATED CONTENT

Ⓢ Supporting Information. ^{1}H and ^{13}C NMR spectra of the newly synthesized compounds and the optical spectra of the compounds recorded in different solvents. This material is available free of charge via the Internet at http://pubs.acs.org.

■ AUTHOR INFORMATION

Corresponding Author
*Tel: +91-1332-285376. Fax: +91-1332-286202. E-mail: krjt8fcy@iitr.ernet.in.

■ ACKNOWLEDGMENT

■ REFERENCES

(1) O'Regan, B.; Grätzel, M. *Nature* **1991**, 353, 737–740.
(2) (a) Unger, E. L.; Ripaud, E.; Leriche, P.; Cravino, A.; Roncali, J.; Johansson, E. M. J.; Hagfeldt, A.; Boschloo, G. *J. Phys. Chem. C* **2010**, *114*, 11659–11667. (b) Liang, Y. L.; Peng, B.; Liang, J.; Tao, Z. L.; Chen, J. *Org. Lett.* **2010**, *12*, 1204–1207. (c) Marinado, T.; Nonomura, K.; Nissfolk, J.; Karlsson, M. K.; Hagberg, D. P.; Sun, L. C.; Mori, S.; Hagfeldt, A. *Langmuir* **2010**, *26*, 2592–2598. (d) Baheti, A.; Tyagi, P.; Thomas, K. R. J.; Hsu, Y. C.; Lin, J. T. *J. Phys. Chem. C* **2009**, *113*, 8541–8547. (e) Li, R. Z.; Lv, X. J.; Shi, D.; Zhou, D. F.; Cheng, Y. M.; Zhang, G. L.; Wang, P. *J. Phys. Chem. C* **2009**, *113*, 7469–7479.

(f) Preat, J.; Michaux, C.; Jacquemin, D.; Perpete, E. A. *J. Phys. Chem. C* **2009**, *113*, 16821–16833. (g) Shen, P.; Liu, Y. J.; Huang, X. W.; Zhao, B.; Xiang, N.; Fei, J. J.; Liu, L. M.; Wang, X. Y.; Huang, H.; Tan, S. T. *Dyes Pigm.* **2009**, *83*, 187–197. (h) Tian, H. N.; Yang, X. C.; Pan, J. X.; Chen, R. K.; Liu, M.; Zhang, Q. Y.; Hagfeldt, A.; Sun, L. C. *Adv. Funct. Mater.* **2008**, *18*, 3461–3468.

(3) (a) Chen, C. H.; Hsu, Y. C.; Chou, H. H.; Thomas, K. R. J.; Lin, J. T.; Hsu, C. P. *Chem.—Eur. J.* **2010**, *16*, 3184–3193. (b) Karim, M. A.; Cho, Y. R.; Park, J. S.; Kim, S. C.; Kim, H. J.; Lee, J. W.; Gal, Y. S.; Jin, S. H. *Chem. Commun.* **2008**, 1929–1931.

(4) (a) Sakuragi, Y.; Wang, X. F.; Miura, H.; Matsui, M.; Yoshida, T. *J. Photochem. Photobiol. A. Chem.* **2010**, *216*, 1–7. (b) Dentani, T.; Kubota, Y.; Funabiki, K.; Jin, J.; Yoshida, T.; Minoura, H.; Miura, H.; Matsui, M. *New J. Chem.* **2009**, *33*, 93–101. (c) Kim, D.; Song, K.; Kang, M. S.; Lee, J. W.; Kang, S. O.; Ko, J. *J. Photochem. Photobiol. A: Chem.* **2009**, *201*, 102–110. (d) Liu, B.; Zhu, W. H.; Zhang, Q.; Wu, W. J.; Xu, M.; Ning, Z. J.; Xie, Y. S.; Tian, H. *Chem. Commun.* **2009**, 1766–1768.

(5) (a) Imoto, K.; Takahashi, K.; Yamaguchi, T.; Komura, T.; Nakamura, J. I.; Murata, K. *Bull. Chem. Soc. Jpn.* **2003**, *76*, 2277–2283. (b) Sayama, K.; Tsukagoshi, S.; Hara, K.; Ohga, Y.; Shinpou, A.; Abe, Y.; Suga, S.; Arakawa, H. *J. Phys. Chem. B* **2002**, *106*, 1363–1371. (c) Sayama, K.; Tsukagoshi, S.; Mori, T.; Hara, K.; Ohga, Y.; Shinpou, A.; Abe, Y.; Suga, S.; Arakawa, H. *Sol. Energy Mater. Sol. Cells* **2003**, *80*, 47–71.

(6) (a) Daeneke, T.; Kwon, T.-H.; Holmes, A. B.; Duffy, N. W.; Bach, U.; Spiccia, L. *Nature Chem.* **2010**, *3*, 211–215. (b) Wang, Z. S.; Cui, Y.; Dan-Oh, Y.; Kasada, C.; Shinpo, A.; Hara, K. *J. Phys. Chem. C* **2008**, *112*, 17011–17017. (c) Wang, Z. S.; Cui, Y.; Dan-Oh, Y.; Kasada, C.; Shinpo, A.; Hara, K. *J. Phys. Chem. C* **2007**, *111*, 7224–7230. (d) Wang, Z. S.; Cui, Y.; Hara, K.; Dan-Oh, Y.; Kasada, C.; Shinpo, A. *Adv. Mater.* **2007**, *19*, 1138–1141.

(7) Hagfeldt, A.; Boschloo, G.; Sun, L.; Kloo, L.; Pettersson, H. *Chem. Rev.* **2010**, *110*, 6595–6663.

(8) (a) Nazeeruddin, M. K.; De Angelis, F.; Fantacci, S.; Selloni, A.; Viscardi, G.; Liska, P.; Ito, S.; Takeru, B.; Grätzel, M. *J. Am. Chem. Soc.* **2005**, *127*, 16835–16847. (b) Grätzel, M. *J. Photochem. Photobiol. A* **2004**, *164*, 3–14.

(9) Xu, W.; Peng, B.; Chen, J.; Liang, M.; Cai, F. *J. Phys. Chem. C* **2008**, *112*, 874–880.

(10) Wu, T.-Y.; Tsao, M.-H.; Chen, F.-L.; Su, S.-G.; Chang, C.-W.; Wang, H.-P.; Lin, Y.-C.; Ou-Yang, W.-C.; Sun, I.-W. *Int. J. Mol. Sci.* **2010**, *11*, 329–353.

(11) Belfield, K. D.; Bondar, M. V.; Hernandez, F. E.; Przhonska, O. V.; Yao, S. *J. Phys. Chem. B* **2007**, *111*, 12723–12729.

(12) Thomas, K. R. J.; Tyagi, P. *J. Org. Chem.* **2010**, *75*, 8100–8111.

(13) (a) Granzhan, A.; Ihmels, H.; Viola, G. *J. Am. Chem. Soc.* **2007**, *129*, 1254–1267. (b) van den Berg, O.; Jager, W. F.; Picken, S. J. *J. Org. Chem.* **2006**, *71*, 2666–2676.

(14) Nazeeruddin, M. K.; Péchy, P.; Renouard, T.; Zakeeruddin, S. M.; Humphry-Baker, R.; Comte, P.; Liska, P.; Cevey, L.; Costa, E.; Shklover, V.; Spiccia, L.; Deacon, G. B.; Bignozzi, C. A.; Grätzel, M. *J. Am. Chem. Soc.* **2001**, *123*, 1613–1624.

(15) Cheng, H. M.; Hsieh, W. F. *Energy Environ. Sci.* **2010**, *3*, 442–447.

(16) Parr, R. G.; Yang, W. T. *Annu. Rev. Phys. Chem.* **1995**, *46*, 701–728.

(17) Lee, C.; Yang, W.; Parr, R. G. *Phys. Rev. B* **1988**, *37*, 785–789.

(18) Yanai, T.; Tew, D. P.; Handy, N. C. *Chem. Phys. Lett.* **2004**, *393*, 51–57.

(19) Lynch, B. J.; Fast, P. L.; Harris, M.; Truhlar, D. G. *J. Phys. Chem. A* **2000**, *104*, 4811–4815.

(20) Lin, S.-H.; Hsu, Y.-C.; Lin, J. T.; Lin, C.-K.; Yang, J.-S. *J. Org. Chem.* **2010**, *75*, 7877–7886.

(21) Grätzel, M. *Nature* **2001**, *414*, 338–344.

(22) Hagfeldt, A.; Grätzel, M. *Chem. Rev.* **1995**, *95*, 49–68. (b) Wang, P.; Zakeeruddin, S. M.; Moser, J.-E.; Grätzel, M. *J. Phys. Chem. B* **2003**, *107*, 13280–13285.

(23) Paek, S.; Choi, H.; Choi, H.; Lee, C.-W.; Kang, M.-S.; Song, K.; Nazeeruddin, M. K.; Ko, J. *J. Phys. Chem. C* **2010**, *114*, 14646–14653.

(24) Hardin, B. E.; Hoke1, E. T.; Armstrong, P. B.; Yum, J.-H.; Comte, P.; Torres, T.; Fréchet, J. M. J.; Nazeeruddin, M. K.; Grätzel, M.; McGehee, M. D. *Nat. Photonics* **2009**, *3*, 406–411.

(25) Zhang, X.-H.; Cui, Y.; Katoh, R.; Koumura, N.; Hara, K. *J. Phys. Chem. C* **2010**, *114*, 18283–13290.

(26) Lagemaat, J.; van de; Park, N.-G.; Frank, A. J. *J. Phys. Chem. B* **2000**, *104*, 2044–2052.

(27) Jeona, S.-H.; Anandakathira, R.; Chianga, J.; Chiang, L. Y. *J. Macromol. Sci., Part A: Pure Appl. Chem.* **2007**, *44*, 1275–1282.

(28) Low, P. J.; Paterson, M. A. J.; Yufit, D. S.; Howard, J. A. K.; Cherryman, J. C.; Tackley, D. R.; Brookc, R.; Brown, B. *J. Mater. Chem.* **2005**, *15*, 2304–2315.

(29) Liu, Q.-D.; Lu, J.; Ding, J.; Tao, Y. *Macromol. Chem. Phys.* **2008**, *209*, 1931–1941.

(30) Frisch, M. J.; Trucks, G. W.; Schlegel, H. B.; Scuseria, G. E.; Robb, M. A.; Cheeseman, J. R.; Scalmani, G.; Barone, V.; Mennucci, B.; Petersson, G. A.; Nakatsuji, H.; Caricato, M.; Li, X.; Hratchian, H. P.; Izmaylov, A. F.; Bloino, J.; Zheng, G.; Sonnenberg, J. L.; Hada, M.; Ehara, M.; Toyota, K.; Fukuda, R.; Hasegawa, J.; Ishida, M.; Nakajima, T.; Honda, Y.; Kitao, O.; Nakai, H.; Vreven, T.; Montgomery, J. A., Jr.; Peralta, J. E.; Ogliaro, F.; Bearpark, M.; Heyd, J. J.; Brothers, E.; Kudin, K. N.; Staroverov, V. N.; Kobayashi, R.; Normand, J.; Raghavachari, K.; Rendell, A.; Burant, J. C.; Iyengar, S. S.; Tomasi, J.; Cossi, M.; Rega, N.; Millam, N. J.; Klene, M.; Knox, J. E.; Cross, J. B.; Bakken, V.; Adamo, C.; Jaramillo, J.; Gomperts, R.; Stratmann, R. E.; Yazyev, O.; Austin, A. J.; Cammi, R.; Pomelli, C.; Ochterski, J. W.; Martin, R. L.; Morokuma, K.; Zakrzewski, V. G.; Voth, G. A.; Salvador, P.; Dannenberg, J. J.; Dapprich, S.; Daniels, A. D.; Farkas, Ö.; Foresman, J. B.; Ortiz, J. V.; Cioslowski, J.; Fox, D. J. Gaussian 09, revision A.02; Gaussian, Inc.: Wallingford, CT, 2009.

(31) Becke, A. D. *J. Chem. Phys.* **1993**, *98*, 1372–1377.

(32) (a) Cossi, M.; Barone, V.; Cammi, R.; Tomasi, J. *Chem. Phys. Lett.* **1996**, *255*, 327–335. (b) Tomasi, J.; Mennucci, B.; Cammi, R. *Chem. Rev.* **2005**, *105*, 2999–3093.